Femtosecond Excitonic Relaxation Dynamics of Perovskite on Mesoporous Films of Al_2O_3 and NiO Nanoparticles**

Hung-Yu Hsu, Chi-Yung Wang, Amir Fathi, Jia-Wei Shiu, Chih-Chun Chung, Po-Shen Shen, Tzung-Fang Guo, Peter Chen, Yuan-Pern Lee, and Eric Wei-Guang Diau

Abstract: The excitonic relaxation dynamics of perovskite adsorbed on mesoporous thin films of Al_2O_3 and NiO upon excitation at 450 nm were investigated with femtosecond optical gating of photoluminescence (PL) via up-conversion. The temporal profiles of emission observed in spectral region 670–810 nm were described satisfactorily with a composite consecutive kinetic model and three transient components representing one hot and two cold excitonic relaxations. All observed relaxation dynamics depend on the emission wavelength, showing a systematic time–amplitude correlation for all three components. When the NiO film was employed, we observed an extent of relaxation proceeding through the nonemissive surface state larger than through the direct electronic relaxation channel, which quenches the PL intensity more effectively than on the Al_2O_3 film. We conclude that perovskite is an effective hole carrier in a p-type electrode for NiO-based perovskite solar cells showing great performance.

The development of all solid-state mesoscopic solar cells attained a new milestone when the devices made of organometallic lead-halide perovskite materials were reported with a power conversion efficiency (PCE) exceeding 15%.[1] The key material, perovskite, acts as a light absorber to harvest sunlight up to 800 nm while the material itself can also act as a transporter of electrons or holes after charge separation.[2] This feature is important for perovskite solar cells to attain such a great device performance, but the fundamental processes governing the operational principle of cells of this type are poorly understood.[3] As Burn and Meredith mentioned,[4] the great performance of these perovskite solar cells seems to combine the advantages of both dye-sensitized solar cells (DSSC) and organic photovoltaics

(OPV), but the mechanism of the carriers (excitons) generated and transported to the electrodes remains unclear.

The dynamics of carrier transport and relaxation in perovskite materials of varied type might provide information crucial for an understanding of the best device architecture in balancing light absorption and charge collection. We demonstrated that perovskite solar cells using mesoporous NiO nanocrystals as a p-contact electrode material in a device configuration NiO/perovskite/PCBM attained PCE 9.5%, giving a promising perspective for further development of all-inorganic perovskite-based thin-film solar cells and tandem photovoltaics.[5] To understand the excitonic relaxation mechanism in the perovskite solar cells, we measured femtosecond photoluminescence (PL) up-conversion for perovskite ($CH_3NH_3PbI_3$) deposited on thin films of nanocrystalline NiO and Al_2O_3 upon excitation at 450 nm.

Both Al_2O_3 and NiO nanocrystalline films were prepared on a glass substrate with spin coating of dispersive solutions containing the corresponding nanoparticles to attain uniform mesoporous films of thickness ca. 500 nm. The $CH_3NH_3PbI_3$ layer was then deposited on those mesoporous films according to procedures reported elsewhere.[1a] Figure 1 shows the

[*] H.-Y. Hsu, C.-Y. Wang, A. Fathi, J.-W. Shiu, C.-C. Chung,
Prof. Dr. Y.-P. Lee, Prof. Dr. E. W.-G. Diau
Department of Applied Chemistry and Institute of Molecular
Science, National Chiao Tung University
Hsinchu 300 (Taiwan)
E-mail: diau@mail.nctu.edu.tw

P.-S. Shen, Prof. Dr. T.-F. Guo, Prof. Dr. P. Chen
Department of Photonics and Advanced Optoelectronic Technology
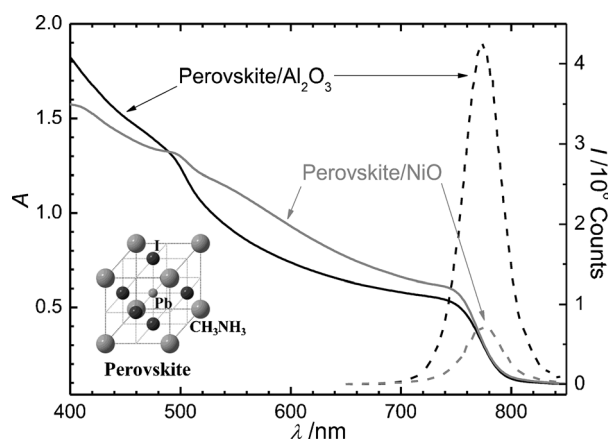Center, National Cheng Kung University
Tainan 701 (Taiwan)

Figure 1. Absorption (solid curves; *A* represents absorbance) and photoluminescence (dashed curves; *I* represents PL intensity) spectra of perovskite/Al_2O_3 (black) and perovskite/NiO (gray) films. The inset shows the chemical structure of a methylammonium lead triiodide perovskite, $CH_3NH_3PbI_3$.

UV/Vis absorption and PL spectra of $CH_3NH_3PbI_3$ on Al_2O_3 and NiO films. The absorption spectra of both films exhibit a continuous feature typical of a perovskite material with band gap energy 1.5 eV.[6] The absorption spectrum of a pure $CH_3NH_3PbI_3$ layer contains two absorption peaks, one at

760 nm corresponding to the direct band gap transition from the first valence band (VB1) to CB and the other at 480 nm to the transition from the second valence band (VB2) to CB.[3b] Our absorption spectrum of the perovskite/Al$_2$O$_3$ film is similar to that of Xing et al. reported in Ref. [3b] for a pure perovskite, indicating a small interaction between the two species. However, the spectrum of the perovskite/NiO film shows a higher absorbance for the VB1–CB transition, and this implies that the interaction between VB1 of perovskite and VB of NiO was significantly enhanced.

With excitation at 450 nm at which both films have similar absorbance, the steady-state PL spectra were recorded under the same experimental conditions (dashed curves in Figure 1). The PL intensity of the perovskite coated on the NiO film was quenched more significantly than that deposited on the Al$_2$O$_3$ film. The PL quenching of the perovskite excitons might be caused by the extraction of the charge carriers across the interface through either an n-type electron-extraction layer (e.g., PCBM) or a p-type hole-extraction layer (e.g., spiro-OMeTAD).[2c,3a,b] As Al$_2$O$_3$ has a large band gap and was treated as an insulating layer for perovskite,[6b] the enhanced quenching of PL for perovskite coated on the p-type NiO film is expected to be the result of an efficient hole extraction across the CH$_3$NH$_3$PbI$_3$/NiO interface, which we discuss below.

Femtosecond PL transients were recorded upon excitation at 450 nm with the emissions probed in the spectral region 670–810 nm. Figure 2a and b show the temporal
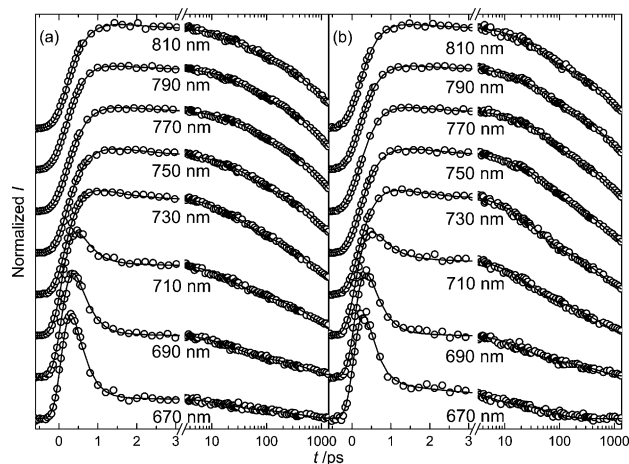

Figure 2. Normalized upconversion photoluminescence transients for thin-film samples of a) perovskite/Al$_2$O$_3$ and b) perovskite/NiO upon excitation at 450 nm and probed at the indicated wavelengths. The circles are experimental data and the solid curves are the fitted results according to a kinetic model explained in the text.

profiles of these PL transients for the Al$_2$O$_3$ and NiO films, respectively. At smaller wavelengths (670–710 nm), all transients involve one rapid-decay component on a scale 0-2 ps with two slow-decay components on time scale 10 ps–1 ns. The contribution of the two slow-decay components becomes more pronounced, and the transients feature a rise-and-decay character, at larger wavelengths (730–810 nm). To ensure that

the observed rapid relaxation was not induced from Auger recombination, power-dependent measurements were performed (Supporting Information, Figure S1).

To understand the rising feature of these transients, we compared two typical transients of perovskite coated on these films in a short period. Figure 3a and b show the PL transients
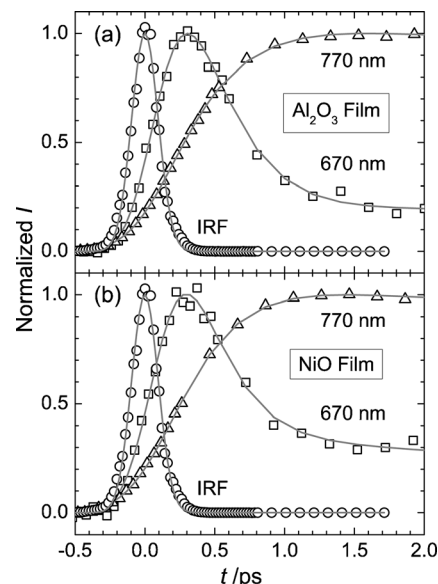

Figure 3. Normalized photoluminescence transient profiles of perovskite deposited on an a) Al$_2$O$_3$ film and a b) NiO film in a range 0–2 ps with probe wavelengths at 670 nm (squares) and 770 nm (triangles); the transient of instrument response function (IRF) shown as circles was obtained from third-harmonic generation (THG) of the gate pulse at 900 nm with the excitation pulse at 450 nm. The solid curves are the fitted results according to a kinetic model explained in the text.

at 670 and 770 nm within the time window 0–2 ps for perovskite coated on Al$_2$O$_3$ and NiO films, respectively; the temporal profiles of the third-harmonic generation (THG) of the fundamental wavelength at 900 nm are shown also to represent the instrument response function (IRF) of the femtosecond pulses. The excitation at 450 nm invokes a transition from VB2 to generate hot excitons in the CB of perovskite;[3b] the probe at 670 nm corresponds to emission from the CB to VB1, as indicated in the schematic picture shown in the left part of Figure 4. We observed unambiguously that the transient at 670 nm involves an intermediate component with a rise-and-decay feature within 1 ps; the transient probed at 770 nm shows only the rising character at this short period. To fit these transients systematically at all wavelengths, we applied a parallel consecutive kinetic model as discussed in the following.

The transients of the two films shown in Figure 2 and 3 were fitted satisfactorily with a kinetic model containing two sequential relaxations in parallel:
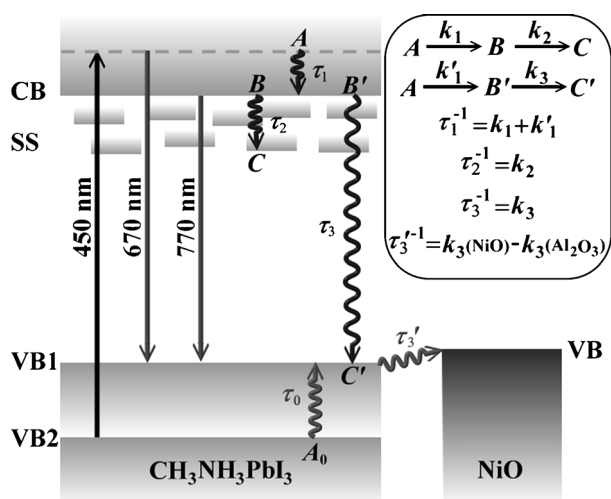
$$A_0 \xrightarrow{k_0} A \xrightarrow{k_1} B \xrightarrow{k_2} C \tag{1}$$

$$A_0 \xrightarrow{k_0} A \xrightarrow{k_1'} B' \xrightarrow{k_3} C' \tag{2}$$

Figure 4. Mechanism of excitonic relaxation showing radiative and non-radiative processes observed for perovskite sensitized on mesoporous semiconductor films. A parallel consecutive kinetic model utilized to fit all PL transients is shown in the top right panel of the scheme. CB: conduction band; VB: valence band; SS: surface state.

Component A_0 represents the hole of $CH_3NH_3PbI_3$ in the VB2 state with a hole cooling rate coefficient k_0, and component A represents hot electrons of $CH_3NH_3PbI_3$ in the CB state with electron cooling rate coefficients k_1 and k_1' to produce components B and B', respectively. Components B and B' represent the two parts of the cold electrons of $CH_3NH_3PbI_3$ in the CB state; one part (B) relaxes to the surface state (SS; C) with an electronic-relaxation rate coefficient k_2 and the other part (B') relaxes to the VB1 state (C') with an electronic-relaxation rate coefficient k_3. Because component A_0 was unobservable in the detection window 670–810 nm (Figure 2), the transients were fitted with a convolution of an IRF (Gaussian) with the kinetic response function containing only three components: A, B and B'.[7] The fitted transients and each corresponding deconvoluted component are shown in Figure S2 and S3, for $CH_3NH_3PbI_3$/Al_2O_3 and $CH_3NH_3PbI_3$/NiO films, respectively; the corresponding fitted parameters are summarized in Table S1 under the conditions $k_0 = k_1 + k_1'$ (or $\tau_0 = \tau_1$) and setting the FWHM of IRF as a free parameter.[8] Figure S4 compares the fitted amplitudes and time coefficients of both films at varied emission wavelengths.

The relaxation mechanism is shown in Figure 4: the excitation at 450 nm pumped the perovskite from the VB2 state to the hot CB state; the emissions probed at 670 and 770 nm correspond to the transitions of hot CB→VB1 and cold CB→VB1, respectively. For component A, the values of amplitude decrease whereas the time coefficients (τ_0 or τ_1) increase as the emission window moves to larger wavelength; the same effect was observed for both metal oxide films, which consolidates the intrinsic transient property for component A. We therefore assign the rise and decay of component A being due to either the hole relaxation from VB2 to VB1 or the hot-electron relaxation in the CB of perovskite, with equal time coefficients, $\tau_0 = 1/k_0$ and $\tau_1 = 1/(k_1 + k_1')$.[8]

For components B and B', the values of their amplitudes increase with the probe wavelength because the detection window at larger wavelength would probe more thermally relaxed perovskite species on both films. The amplitudes of component B are greater on the NiO film than on the Al_2O_3 film, and vice versa for the component B'. The values of the decay coefficient of component B ($\tau_2 = 1/k_2$) are similar for both films, but the values of the decay coefficient of component B' ($\tau_3 = 1/k_3$) of the Al_2O_3 film are significantly greater than those of the NiO film. The relaxation times $\tau_2 = 20$–50 ps are consistent with those observed on Al_2O_3 and TiO_2 films using the fs-TAS method.[3d,6a] We thus assign component B as part of the cold excitons in the CB of perovskite relaxing to the non-emissive surface state with a surface-state relaxation time τ_2, and component B' as another part of the cold excitons inside perovskite via internal conversion from CB to VB1 with a bulk-state electronic relaxation time τ_3. Because the amplitudes of component B are greater on the NiO film than on the Al_2O_3 film, the observed quenching of the steady-state PL intensity of perovskite shown in Figure 1 might be attributed to the surface-state relaxation of perovskite, which is more significant for the NiO film than for the Al_2O_3 film. The surface-state relaxation times were observed to be the same for both Al_2O_3 and NiO films, indicating that this intrinsic relaxation occurs on the surface of the perovskite.

The contact of perovskite with the NiO film in a mesoscopic environment might create more surface states than with the Al_2O_3 film, as we observed here. Surface states in semiconducting solar cells typically cause efficient charge recombination and yield poor photovoltaic performance. In the case of perovskite solar cells, however, excitons in the surface states of perovskite might have greater lifetimes to sustain a charge separation better in the interface between perovskite and electron- or hole-transporting layer. The kinetics involving the excitonic relaxation of perovskite in the non-emissive surface states should be further investigated using other time-resolved spectral techniques.[3b,d,6a]

Distinct relaxation times in τ_3 were observed for both films; the bulk-state relaxation of perovskite on the NiO film was more rapid than that on the Al_2O_3 film. Treating the insulating Al_2O_3 film as a reference, we attribute the observed decreased relaxation times (τ_3) of the NiO film to the contribution of hole transport at the interface between the VB1 of perovskite and the VB of NiO with time coefficient τ_3'. We estimated the values of τ_3' at emission wavelengths 690-810 nm on subtracting the decay coefficients of component B' (τ_3^{-1}) of the NiO film from that of the Al_2O_3 film; the results appear in Figure S5. The interfacial hole transport in the $CH_3NH_3PbI_3$/NiO interface is derived to be on a time scale 5 ns, which is much greater than that reported for a $CH_3NH_3PbI_3$/Spiro-OMeTAD system (0.66 ns).[3b] The electron-extraction time at the perovskite/PCBM interface was reported, however, to occur on the scale of 0.4 ns,[3b] which is much smaller than the hole-extraction time that we observed in the perovskite/NiO interface. Perovskite itself can hence serve as a hole carrier with a sufficient lifetime to reach the p-contact material.

In a recent report on excitation of the perovskite/NiO film at 460 nm,[5] we observed the formation of cationic species NiO$^+$ appearing in the spectral region 900–1500 nm using photo-induced absorption (PIA) spectra. This important evidence indicates that charge separation does occur in the perovskite/NiO interface within the observed period 5 ns. It is interesting to note that surface states created in the perovskite/NiO interface quenched the PL intensity of perovskite significantly but they did not deteriorate the device performance; a NiO-based p-type mesoscopic perovskite solar cell was reported to attain a remarkable device performance with PCE 9.5 %.[5]

In conclusion, we report here our investigation of the relaxation dynamics of perovskite sensitized on NiO and Al$_2$O$_3$ films using femtosecond optical gating upon excitation at 450 nm. The PL transients of the two films observed in spectral region 670–810 nm all feature three wavelength-dependent transient components in a composite consecutive kinetic model involving hot-hole cooling from VB2 to VB1 (0.2–0.5 ps), hot-electron relaxation in CB (0.2–0.5 ps), surface-state excitonic relaxation from CB to SS (20–50 ps) and bulk-state internal conversion from CB to VB1 (0.5–1.2 ns). The enhanced quenching of PL of perovskite on NiO with respect to that on Al$_2$O$_3$ is due to the exciton relaxation to the non-emissive surface state, which is more significant for the NiO film than for the Al$_2$O$_3$ film. We observed the hole-extraction interval at the perovskite/NiO interface to be 5 ns at the PL maximum (770 nm), which is much greater than observed in other organic systems probed at 760 nm.[3b] The p-type device with the NiO/perovskite/PCBM film configuration exhibiting remarkable photovoltaic performance[5] thus indicates that perovskite itself can serve as an effective hole transporter after charge separation at the perovskite/PCBM interface. Our investigation thus establishes a concrete kinetic model to understand the excitonic relaxation dynamics of perovskite in varied film configurations.

[1] a) J. Burschka, N. Pellet, S. J. Moon, R. Humphry-Baker, P. Gao, M. K. Nazeeruddin, M. Grätzel, *Nature* **2013**, *499*, 316; b) M. Liu, M. B. Johnston, H. J. Snaith, *Nature* **2013**, *501*, 395; c) D. Liu, T. L. Kelly, *Nat. Photonics* **2014**, *8*, 133; d) J. T. W. Wang, et al., *Nano Lett.* **2014**, *14*, 724; e) J. H. Rhee, C. C. Chung, E. W. G. Diau, *NPG Asia Mater.* **2013**, *5*, e68; f) H. J. Snaith, *J. Phys. Chem. Lett.* **2013**, *4*, 3623.

[2] a) L. Etgar, P. Gao, Z. Xue, Q. Peng, A. K. Chandiran, B. Liu, Md. K. Nazeeruddin, M. Grätzel, *J. Am. Chem. Soc.* **2012**, *134*, 17396; b) J. Y. Jeng, Y. F. Chiang, M. H. Lee, S. R. Peng, T. F. Guo, P. Chen, T. C. Wen, *Adv. Mater.* **2013**, *25*, 3727; c) P. Docampo, J. M. Ball, M. Darwich, G. E. Eperon, H. J. Snaith, *Nat. Commun.* **2013**, *4*, 2761.

[3] a) S. D. Stranks, G. E. Eperon, G. Grancini, C. Menelaou, M. J. P. Alcocer, T. Leijtens, L. M. Herz, A. Petrozza, H. J. Snaith, *Science* **2013**, *342*, 341; b) G. Xing, N. Mathews, S. Sun, S. S. Lim, Y. M. Lam, M. Grätzel, S. Mhaisalkar, T. C. Sum, *Science* **2013**, *342*, 344; c) C. Wehrenfennig, G. E. Eperon, M. B. Johnston, H. J. Snaith, L. M. Herz, *Adv. Mater.* **2014**, *26*, 1584; d) A. Marchioro, J. Teuscher, D. Friedrich, M. Kunst, R. van de Krol, T. Moehl, M. Grätzel, J. E. Moser, *Nat. Photonics* **2014**, *8*, 250; e) V. Roiati, S. Colella, G. Lerario, L. De Marco, A. Rizzo, A. Listorti, G. Gigli, *Energy Environ. Sci.* **2014**, *7*, 1889.

[4] P. L. Burn, P. Meredith, *NPG Asia Mater.* **2014**, *6*, e79.

[5] K. C. Wang, et al., *Sci. Rep.* **2014**, *4*, 4756.

[6] a) H. S. Kim, et al., *Sci. Rep.* **2012**, *2*, 591; b) M. M. Lee, J. Teuscher, T. Miyasaka, T. N. Murakami, H. J. Snaith, *Science* **2012**, *338*, 643.

[7] a) Y. C. Lu, C. W. Chang, E. W. G. Diau, *J. Chin. Chem. Soc.* **2002**, *49*, 693; b) Y. C. Lu, E. W. G. Diau, H. Rau, *J. Phys. Chem. A* **2005**, *109*, 2090; c) L. Luo, C. F. Lo, C. Y. Lin, I J. Chang, E. W. G. Diau, *J. Phys. Chem. B* **2006**, *110*, 410.

[8] The quality of the fit was poor when the FWHM of the IRF was fixed at 200 fs according to the THG signals, but perfect fits were obtained when the FWHM was set as a free parameter. The values of the fitted IRF increase upon increasing the wavelength (Table S1), which cannot be explained as the result of group velocity dispersion (GVD). The PL transients featuring with a rise character indicate the necessity of using a consecutive kinetic model for the fit. However, the hot-hole cooling (represented by a rise in the model) and the hot-electron cooling (represented by a decay in the model) processes should occur simultaneously and we do not have the spectral selectivity to distinguish between the hot electrons and the hot holes as long as the spectral gap between these two species matches our probe window at a certain PL wavelength. As a result, the hot-hole cooling time (either τ_0 or τ_1) and the hot-electron cooling time (either τ_1 or τ_0) were setting to be equal ($\tau_0 = \tau_1$). Setting IRF as a free parameter is thus to give more freedom for the fit to compensate the dynamic effect of thermalization for both hot holes and electrons in an average way according to the composite consecutive kinetic model proposed herein.